

# Solid-state Circuit Breaker Based on Cascaded Normally-on SiC JFETs for Medium-voltage DC Distribution Networks

Dong He, *Member, IEEE*, Haohui Zhou, Zheng Lan, *Member, IEEE*, Wei Wang, *Student Member, IEEE*, Jinhui Zeng, *Member, IEEE*, Xueping Yu, and Z. John Shen, *Fellow, IEEE*

**Abstract**—Solid-state circuit breakers (SSCBs) are critical components in the protection of medium-voltage DC distribution networks to facilitate arc-free, fast and reliable isolation of DC faults. However, limited by the capacity of a single semiconductor device, using semiconductor-based SSCBs at high voltage is challenging. This study presents the details of a 1.5 kV, 63 A medium-voltage SSCB, composed primarily of a solid-state switch based on three cascaded normally-on silicon carbide (SiC) junction field-effect transistors (JFETs) and a low-cost programmable gate drive circuit. Dynamic and static voltage sharing among the cascaded SiC JFETs of the SSCB during fault isolation is realized using the proposed gate drive circuit. The selection conditions for the key parameters of the SSCB gate driver are also analyzed. Additionally, an improved pulse-width modulation current-limiting protection solution is proposed to identify the permanent overcurrent and transient inrush current associated with capacitive load startup in a DC distribution network. Using the developed SSCB prototype and the fault test system, experimental results are obtained to validate the fault response performance of the SSCB.

**Index Terms**—Solid-state circuit breaker, DC distribution network, SiC JFET, voltage balancing, inrush current.

## I. INTRODUCTION

The rapid development of power semiconductor devices and distributed power-generation technologies [1] has led to significant interest in DC power distribution in both academic and industrial circles [2], [3]. However, DC distribution networks have low-impedance characteristics with large DC-link capacitors. Consequently, when a DC short-circuit fault occurs, the peak value of the fault current can be very

high, with no natural zero crossing [4]. Thus, further research and development of DC circuit breakers with rapid response are key to the promotion of applications for DC distribution.

Solid-state circuit breakers (SSCBs) that use power semiconductor devices as breaking elements have attracted significant research attention because of their advantages, including fast response, flexible controllability, and arc-free switching [5]–[7]. Recently, numerous novel wide-bandgap (WBG) semiconductor devices have been developed, such as silicon carbide (SiC) metal-oxide semiconductor field-effect transistors (MOSFETs), SiC junction field-effect transistors (JFETs), and SiC static induction transistors (SITs). These SiC power devices have small ON-state resistance, wide safe operating area, and fast switching speed [8–10]. Thus, they are excellent candidates for the development of fast-response SSCBs [11]–[16]. In [11], a low-voltage 400 V SSCB based on SiC SITs is used in a DC distribution system. It effectively reduces the over-voltage of the circuit breaker during fault isolation. Reference [12] develops an 850 V, 100 A circuit breaker using a hybrid power module composed of 1200 V SiC MOSFETs, SiC Schottky diodes, and SiC avalanche breakdown diodes, while in [13], a bidirectional 600 V, 60 A SSCB is proposed using SiC JFETs as static switches. A suitable gate drive circuit for normally-on SiC JFETs is designed to realize DC short-circuit fault protection within a few microseconds [14]. In our previous studies, ultrafast self-powered SSCBs based on normally-on SiC JFETs were reported in [15], [16]. These SSCBs are easy to install as traditional AC air circuit breakers, and the response time is within 10  $\mu$ s. However, the aforementioned SSCB solutions focus primarily on low-voltage applications ranging from 400 V to 1000 V, but do not meet the requirements for high and medium voltage levels.

Considering the technological limitations of SiC power devices, the nominal voltage of a single commercial SiC device produced by companies such as Infineon, Cree, and UnitedSiC is primarily limited to 1200 V. To increase the voltage level of SiC-based SSCBs, the SiC

---

Received: February 26, 2023

Accepted: November 1, 2023

Published Online: March 1, 2024

Zheng Lan (corresponding author) is with the College of Electrical and Information Engineering, Hunan University of Technology, Zhuzhou 412007, China (e-mail: hd861116@163.com).

DOI: 10.23919/PCMP.2023.000143

devices in the main static switches must be connected in series to increase their operational voltage levels [17]. When SiC devices are operated in series, influencing factors such as device parameter differences, drive-signal delay, and asymmetry in circuit design can cause unbalanced voltage distribution, which can significantly hinder the safe operation of the SiC devices. Therefore, the dynamic and static voltage balance in series-connected SiC devices is an important issue that must be addressed.

For the voltage balance problem caused by the series arrangement of SiC devices, single-gate drive circuit methods have been proposed to control the turn-on and turn-off states of cascaded SiC devices [18]–[21]. Reference [18] proposes a voltage-balancing method for a super cascade based on 1200 V SiC JFETs and a low-voltage Si MOSFET. This achieves static and dynamic voltage balancing using single MOSFET gate control and an auxiliary circuit. In [19], a voltage balance control method for SiC MOSFET series circuits is presented, in which only the gate of the bottom SiC MOSFET in the series devices is controlled by the circuit, whereas the remaining SiC MOSFETs are controlled using an external power source and an auxiliary circuit. However, the use of a power supply significantly increases the volume and losses of the control system. In [20], a gate-control method suitable for SiC MOSFET series operation based on a snubber circuit is proposed. However, the static voltage balancing needs further improvement. In terms of series connection of normally-on SiC JFETs, reference [21] uses a Zener diode and an  $RC$  circuit to achieve voltage balancing during SiC JFET cascade operation, thereby increasing the operational voltage of the SSCB. However, this method causes a proportional increase in the number of Zener diodes when the number of series devices increases, which significantly increases the circuit loss. Furthermore, the SSCB only responds to faults with fault current being 4 times or more of the SiC JFET nominal current. In this case, such a high overcurrent is likely to damage the main SiC JFET switches because of overheating. A single-gate driver-cascaded SiC JFETs with an active clamp circuit for a medium-voltage SSCB is proposed in [22], [23]. The complexity of the gate drive circuit is reduced, and the voltage overshoots of the SiC JFETs in series are effectively reduced during SSCB operation. However, more passive components have to be used in this method, and the losses of the drive circuit increase with the increase of the SiC JFETs. Also, the impact of the inrush current generated on the SSCB during capacitive load startup is not considered. Therefore, for a SiC-based SSCB to meet the requirements of medium-voltage operation, a gate drive circuit is necessary to achieve a reliable voltage balance for the SiC series circuit to isolate DC faults quickly and reliably. A cascaded SiC-based SSCB using a simple voltage bal-

ancing method and an effective protection strategy is a reasonable option for medium-voltage DC protection.

Previously, we have presented a novel medium-voltage SiC-based SSCB method based on this concept [24]. In this study, the gate drive circuit of the SSCB is further optimized and the operating principles, parameter design considerations, protection schemes, and experimental results of a medium-voltage DC SSCB based on cascading normally-on SiC JFETs are discussed. The main contributions of this paper are:

1) A new voltage-balanced gate drive circuit for medium-voltage SSCB is proposed based on three cascaded normally-on SiC JFETs using the principle of capacitive coupling. This method only requires an external drive signal for the bottom SiC JFET in a series circuit to control the turn-on and turn-off of the SSCB. Thus, improved dynamic and static voltage balancing can be achieved during fault isolation.

2) An improved pulse-width modulation (PWM) current-limiting protection scheme for the SSCB is presented to identify short circuits (4 times or more of the SiC JFET nominal current), overcurrent (2 or 3 times of the SiC JFET nominal current), and inrush current (generated by capacitive loading), which ensures high-quality and reliable operation of the DC distribution network. In addition, during overcurrent protection, the thermal stress of the SiC JFETs in the SSCB main switch is significantly reduced.

The remainder of this paper is organized as follows: Section II presents the operational principles of the novel voltage-balanced circuit for the medium-voltage SSCB, while Section III discusses the selection criteria for the key parameters in the SSCB gate drive circuit obtained via analysis and derivation of the circuit. Section IV demonstrates the improved PWM current-limiting protection scheme for achieving fast DC short circuit and overcurrent fault protection. In Section V, the experimental evaluation of the new SSCB design method is presented, and Section VI presents the main conclusions of the paper.

## II. PROPOSED SSCB BASED ON CASCADED SiC JFETs

### A. Structure and Principle of SSCB

In this study, by exploiting the advantages of normally-on SiC JFET devices, a programmable gate drive circuit of cascaded SiC JFETs is proposed for SSCB, as shown in Fig. 1. In the SSCB, the current and voltage sampling circuits transmit the current  $i_d$  flowing through the drain of the SiC JFETs and the load-side voltage  $V_o$  to the microprocessor. The two sampled  $i_d$  and  $V_o$  signals can be used to determine whether short-circuit or overcurrent faults occur in the medium-voltage DC system using a programmable gate-drive circuit, in combination with a fault-protection method.

Finally, the SSCB protects according to the type of DC fault to achieve rapid fault isolation. The DC bus serves as a working power supply directly for the drive circuit using a step-down isolated DC/DC converter, thus eliminating the need for an additional auxiliary power supply and reducing the size of the SSCB. The basic structure and operating principles of the SSCB are described in the following sections.

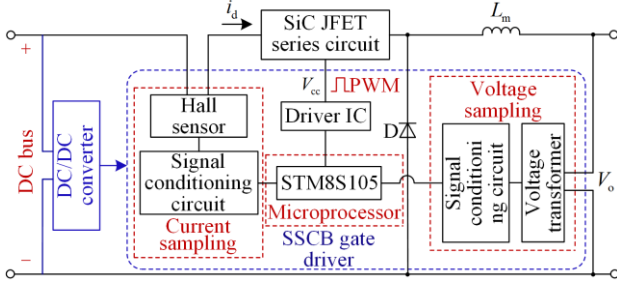


Fig. 1. Simplified schematic diagram of the proposed SSCB.

### 1) Signal Sampling Circuit

This circuit is composed primarily of current- and voltage-sampling circuits. In the case of a short circuit or an overcurrent fault,  $i_d$  flows through the drain of the series-connected SiC JFETs in the SSCB. At this point, the current-sampling circuit uses a fast-response Hall sensor to transmit  $i_d$  to the signal-conditioning circuit for processing, and its current value determines the turn-on and turn-off states of the SSCB. When capacitive loading occurs in a DC distribution network, an inrush current is generated, so the SSCB must effectively identify permanent overcurrent faults and inrush current to prevent maloperation. In the voltage-sampling circuit, a voltage transformer is used to detect the load-side voltage  $V_o$ . This voltage signal is processed by a signal-conditioning circuit and is then transmitted to the microprocessor. This is the basis for distinguishing between the overcurrent and inrush current to improve protection reliability.

### 2) Microprocessor Control Unit

The selected microprocessor (STM8S105) in this study is chosen as a compromise between its cost and the data-handling capacity of the fault signals. Combined with the proposed PWM current-limiting protection method, the microprocessor can quickly process the voltage and current signals of the sampling circuit to identify overcurrent and short-circuit faults. Based on the different fault types, a drive control signal is applied to the gate of the SiC JFETs to isolate the faults. Compared with the SSCB and the fault protection methods proposed in [15], the use of the microprocessor facilitates the reliable identification of overcurrents and inrush currents in DC systems. Further, improved efficacy of the SSCB can be realized by designing corresponding protection methods based on the different fault types.

### 3) SiC JFET Series Circuit

The SiC JFET series circuit is composed primarily of three normally-on SiC JFETs ( $J_1$ ,  $J_2$ , and  $J_3$ ) connected in series, as shown in Fig. 2. To reduce the influence of the gate drive signal delay or the drive resistance difference on the voltage balance of the cascaded SiC JFETs, a standard gate drive circuit is designed to control the turn-on and turn-off of all the SiC JFETs. In addition, an  $RC$  voltage snubber circuit is connected in parallel between the drain and source of each SiC JFET to achieve dynamic voltage balance of the SiC JFETs, while resistors  $R_1$ ,  $R_2$ , and  $R_3$  are used to improve the static voltage sharing of the SiC JFETs. Assuming that the microprocessor recognizes a short circuit in the DC network, it sends a trigger signal  $V_{cc}$  ( $-15$  V) to the bottom device  $J_1$ . At this time,  $J_1$  is turned off and its drain-source voltage gradually increases. When the gate-source voltage of  $J_2$  reaches the clamping voltage  $V_{cc}$  of diode  $D_1$  during fast charging of capacitor  $C_1$ ,  $J_2$  is turned off. Similarly, during the turn-off transient of  $J_2$ , the circuit composed of capacitor  $C_2$ , resistor  $R_{g3}$ , and diode  $D_2$  triggers  $J_3$  to the turn-off state. Thus, the three cascaded SiC JFET devices are turned off individually, and short-circuit fault isolation is realized. In the following sections, the turn-off and turn-on processes of an SSCB based on cascaded SiC JFETs are described in detail.

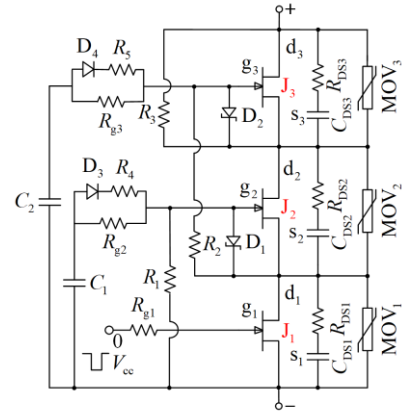


Fig. 2. Structure diagram of the proposed SiC JFET series circuit.

### B. Analysis of the SSCB Turn-off Process

In the event of a short circuit or overcurrent, the circuit breaker gate driver immediately processes the current signal  $i_d$  and voltage signal  $V_o$ , and sends a trigger signal  $V_{cc}$  ( $-15$  V) to the gate of the cascaded SiC JFETs to interrupt the fault current. The typical voltage and current waveforms of the cascaded SiC JFETs when the SSCB is turned off are depicted in Fig. 3, and the corresponding critical currents are illustrated in Fig. 4. At

time  $t_0$ , the initial conditions of the DC network are expressed as follows:

$$\begin{cases} V_{gs-J1}(t_0) = V_{gs-J2}(t_0) = V_{gs-J3}(t_0) = 0 \\ I_{D-J1}(t_0) = I_{D-J2}(t_0) = I_{D-J3}(t_0) = I_o \\ V_{ds-J1}(t_0) = V_{ds-J2}(t_0) = V_{ds-J3}(t_0) = I_o R_{DS,on} \end{cases} \quad (1)$$

where  $V_{gs-J1}$ ,  $V_{gs-J2}$ ,  $V_{gs-J3}$ ,  $V_{ds-J1}$ ,  $V_{ds-J2}$ ,  $V_{ds-J3}$  are the gate-source voltages and drain-source voltages across  $J_1$ ,  $J_2$ , and  $J_3$  in the SSCB main switch, respectively;  $I_{D-J1}$ ,  $I_{D-J2}$ , and  $I_{D-J3}$  are the drain currents that flow through  $J_1$ ,  $J_2$ , and  $J_3$ , respectively;  $I_o$  represents the load current flowing through the SSCB and the ON-state resistance of the SiC JFETs is defined as  $R_{DS,on}$ .

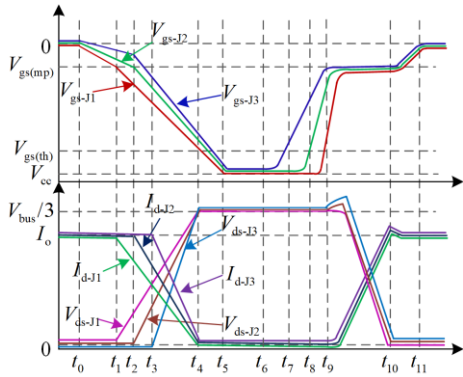


Fig. 3. Idealized voltage and current waveforms of the turn-off and turn-on process for cascaded SiC JFETs.

Stage 1 [ $t_0 - t_1$ ]: assuming that a short circuit occurs at time  $t_0$ , the microprocessor generates a drive voltage ( $V_{cc} = -15$  V) to  $J_1$  to enable the SSCB to interrupt the fault current. At this point,  $V_{cc}$  charges the gate-source capacitor  $C_{gs1}$  via the gate resistor  $R_{g1}$ . The charging current  $i_1$  is shown in Fig. 4(a). Subsequently,  $V_{gs-J1}$  gradually increases in the reverse direction from zero. At time  $t_1$ ,  $V_{gs-J1}(t_1)$  is equal to the Miller plateau voltage  $V_{gs(mp)}$ . During this process,  $I_{D-J2}$ ,  $I_{D-J3}$ ,  $V_{ds-J1}$ ,  $V_{ds-J2}$ ,  $V_{ds-J3}$  are almost constant. The expression for  $V_{gs-J1}(t)$  in this process is given as:

$$V_{gs-J1}(t) = V_{cc}(1 - e^{-t/\tau_1}) \quad (2)$$

$$\tau_1 = R_{g1}(C_{gs1} + C_{gd1}) = R_{g1}C_{iss1} \quad (3)$$

where  $C_{gd1}$  is the gate-drain capacitor of  $J_1$ ;  $C_{iss1}$  is the equivalent input capacitance of the gate of  $J_1$ ; and  $\tau_1$  is the time constant of  $R_{g1}C_{iss1}$  circuit. By introducing  $V_{gs-J1}(t_1) = V_{gs(mp)}$  into (2), the turn-off delay  $\Delta t_1$  can be obtained as:

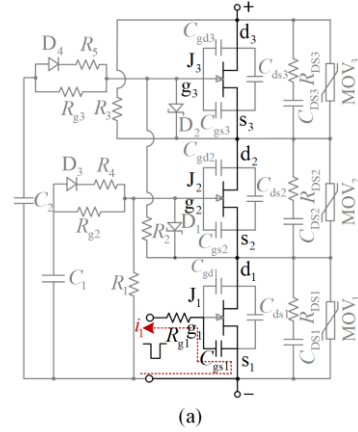
$$\Delta t_1 = t_1 - t_0 = R_{g1}(C_{gs1} + C_{gd1}) \ln \left( \frac{-V_{cc}}{V_{gs(th)} - V_{cc} + I_o / g_m} \right) \quad (4)$$

where  $g_m$  and  $V_{gs(th)}$  are the transconductance and the gate threshold voltage of the SiC JFET, respectively.

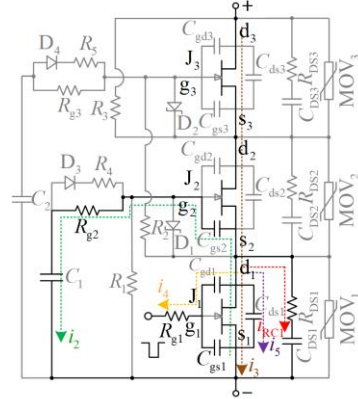
Considering the current-balancing effect in the series circuit, a small leakage current  $i_5$  in the gate circuit of  $J_2$  charges  $C_1$  and  $C_{gs2}$  via  $R_{g2}$  at this stage, as depicted in Fig. 4(b). Therefore,  $I_{D-J1}$  decreases slowly and  $V_{ds-J1}$  satisfies the following relationship:

$$V_{ds-J1} = V_{C1} + V_{Rg2} + V_{Cgs2} \quad (5)$$

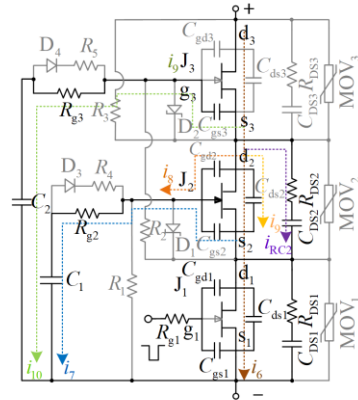
where  $V_{C1}$ ,  $V_{Rg2}$ , and  $V_{Cgs2}$  are the voltages of  $C_1$ ,  $R_{g2}$ , and the gate-source capacitor  $C_{gs2}$ , respectively.



(a)



(b)



(c)

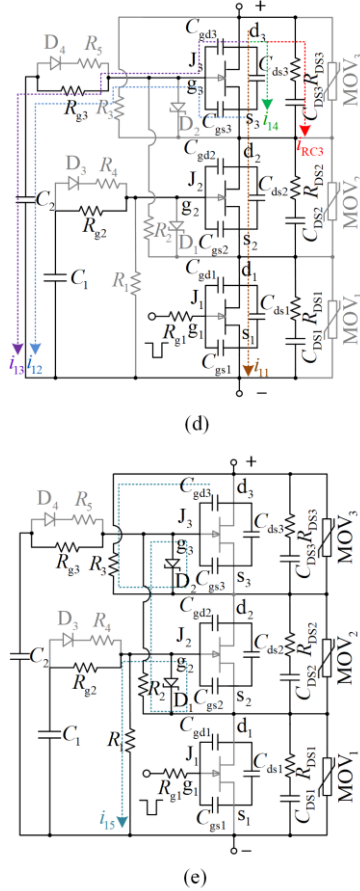


Fig. 4. Main currents of the SiC JFET series circuit during the turn-off process. (a) Stage 1:  $i_1$ . (b) Stage 2:  $i_2$ ,  $i_3$ ,  $i_4$ ,  $i_5$  and  $i_{RC1}$ . (c) Stage 3:  $i_6$ ,  $i_7$ ,  $i_8$ ,  $i_9$ , and  $i_{RC2}$ . (d) Stage 4:  $i_{11}$ ,  $i_{12}$ ,  $i_{13}$ ,  $i_{14}$ , and  $i_{RC3}$ . (e) Stage 5:  $i_{15}$ .

Stage 2 [ $t_1 - t_2$ ]: at time  $t_1$ , when  $V_{gs-J1}$  is equal to the Miller plateau voltage  $V_{gs(mp)}$ ,  $I_{D-J1}$  gradually decreases from  $I_0$ . At this time,  $C_{ds1}$  and  $C_{gd1}$  are charged by  $i_3$  and  $i_4$ , respectively.  $V_{ds-J1}$  increases further, and its rising rate can be approximated as:

$$\frac{dV_{ds-J1}}{dt} \approx -\frac{i_4}{C_{gd1}} = \frac{V_{gs-J1} - V_{cc}}{R_{g1}C_{gd1}} \quad (6)$$

Under the influence of the SiC series circuit,  $I_{D-J2}$  also decreases gradually from  $I_0$ . At the same time, the reverse charging process of the gate-source capacitor  $C_{gs2}$  of  $J_2$  is accelerated by the increase in  $V_{ds-J1}$ , and (5) is still satisfied. Thus,  $V_{gs-J2}$  gradually decreases based on the first stage. The flow paths of the main currents  $i_2$ ,  $i_3$ ,  $i_4$ ,  $i_5$ , and  $i_{RC1}$  during this stage are shown in Fig. 4(b).

Stage 3 [ $t_2 - t_3$ ]: considering that charging of  $C_{gs2}$  has started in the previous stage,  $V_{gs-J2}$  increases from zero to  $V_{gs(mp)}$  at time  $t_2$ . At this stage, the increase in

$V_{ds-J1}$  accelerates the charging process of  $C_{gs2}$ . According to (6), the rate of increase of  $V_{ds-J2}$  is greater than that of  $V_{ds-J1} \cdot C_{ds2}$  and  $C_{gd2}$  of  $J_2$  are charged by  $i_8$  and  $i_9$ , respectively. The flow paths of  $i_6$ ,  $i_7$ ,  $i_8$ ,  $i_9$ , and  $i_{RC2}$  are shown in Fig. 4(c).

In addition to the increase in  $V_{ds-J2}$ , the voltage of the gate-source capacitor  $C_{gs3}$  of  $J_3$  also gradually increases from zero in the reverse direction. Thus, the following relationship can be obtained for the gate circuit of  $J_3$ :

$$V_{C2} + V_{Rg3} + V_{Cgs3} = V_{ds-J1} + V_{ds-J2} \quad (7)$$

where  $V_{C2}$ ,  $V_{Rg3}$ , and  $V_{Cgs3}$  are the voltages associated with  $C_2$ ,  $R_{g3}$ , and the gate-source capacitor  $C_{gs3}$ , respectively.

Stage 4 [ $t_3 - t_4$ ]: during the rapid charging of  $C_{gs3}$  in Stage 3,  $V_{gs-J3}$  increases to  $V_{gs(mp)}$  at time  $t_3$ . Similarly,  $V_{ds-J3}$  further increases owing to the charging of  $C_{ds3}$  and  $C_{gd3}$  by  $i_{13}$  and  $i_{14}$ , respectively. At time  $t_4$ ,  $V_{gs-J1}$ ,  $V_{gs-J2}$ , and  $V_{gs-J3}$  gradually increase to the gate threshold voltage  $V_{gs(th)}$ , and the drain currents  $I_{D-J1}$ ,  $I_{D-J2}$ , and  $I_{D-J3}$  decrease to zero. The drain-source voltages  $V_{ds-J1}$ ,  $V_{ds-J2}$ , and  $V_{ds-J3}$  of all the series devices increase to one-third of  $V_{bus}$ . The path diagrams for  $i_{11}$ ,  $i_{12}$ ,  $i_{13}$ ,  $i_{14}$ , and  $i_{RC3}$  at this stage are shown in Fig. 4(d).

Stage 5 [ $t_4 - t_5$ ]: in this stage,  $V_{gs-J1}$ ,  $V_{gs-J2}$ , and  $V_{gs-J3}$  reverse increase from zero to the bias voltage  $V_{cc} (-15 \text{ V})$ . All cascaded devices are in the off state, and the SiC JFETs are completely turned off, there is only a very small leakage current  $i_{15}$  flowing through the SSCB as shown in Fig. 4(e). Considering that the equivalent resistances of  $J_1$ ,  $J_2$ , and  $J_3$  are much larger than those of  $R_1$ ,  $R_2$ , and  $R_3$  after they are completely turned off, no leakage current flows through the SiC JFETs. The static voltage balance between the series-connected SiC JFETs in the cutoff state is maintained by  $R_1$ ,  $R_2$ , and  $R_3$ , i.e.,  $V_{ds-J1}$ ,  $V_{ds-J2}$ ,  $V_{ds-J3}$  are one-third of the DC-bus voltage  $V_{bus}$ .

### C. Analysis of the SSCB Turn-on Process

If a short circuit or an overcurrent in the DC network is completely cleared, the SSCB changes from the off state to the on state. The voltage and current waveforms during the turn-on transition of the cascaded SiC JFETs are shown in Fig. 3, while the corresponding critical currents are shown in Fig. 5. At time  $t_6$ , the initial condition of the DC system is assumed to be:

$$\begin{cases} V_{gs-J1}(t_6) = V_{gs-J2}(t_6) = V_{gs-J3}(t_6) = V_{cc} \\ I_{D-J1}(t_6) = I_{D-J2}(t_6) = I_{D-J3}(t_6) = 0 \\ V_{ds-J1}(t_6) = V_{ds-J2}(t_6) = V_{ds-J3}(t_6) = V_{bus}/3 \end{cases} \quad (8)$$

Stage 6 [ $t_6 - t_7$ ]: when the fault in the DC network is cleared, the gate voltage  $V_{cc}$  increases from  $-15$  V to  $0$  V at time  $t_6$ , causing the SSCCB to turn on. The voltage  $V_{cc}$  on the gate-source capacitor  $C_{gs1}$  of  $J_1$  is discharged in reverse through  $R_{g1}$ , and the discharge current  $i'_1$  is depicted in Fig. 5(a). Subsequently,  $V_{gs-J1}$  starts increasing from  $-15$  V and reaches the threshold voltage  $V_{gs(th)}$  at time  $t_7$ . During this process, the cascaded devices  $J_1$ ,  $J_2$ , and  $J_3$  are still in the off state. Simultaneously, the gate-source voltages  $V_{gs-J2}$  and  $V_{gs-J3}$  are stable at  $-15$  V, i.e., the drain-source voltages  $V_{ds-J1}$ ,  $V_{ds-J2}$ , and  $V_{ds-J3}$  remain unchanged. The relationship between  $V_{gs-J1}(t)$  and  $V_{cc}$  during this process is given as:

$$V_{gs-J1}(t) = V_{cc} e^{-t/\tau_1} \quad (9)$$

Combining  $V_{gs-J1}(t_7) = V_{gs(th)}$  with (9), the turn-on delay time  $\Delta t_2$  is given by:

$$\Delta t_2 = t_7 - t_6 = R_{g1} (C_{gs1} + C_{gd1}) \ln \left( \frac{V_{cc}}{V_{gs(th)}} \right) \quad (10)$$

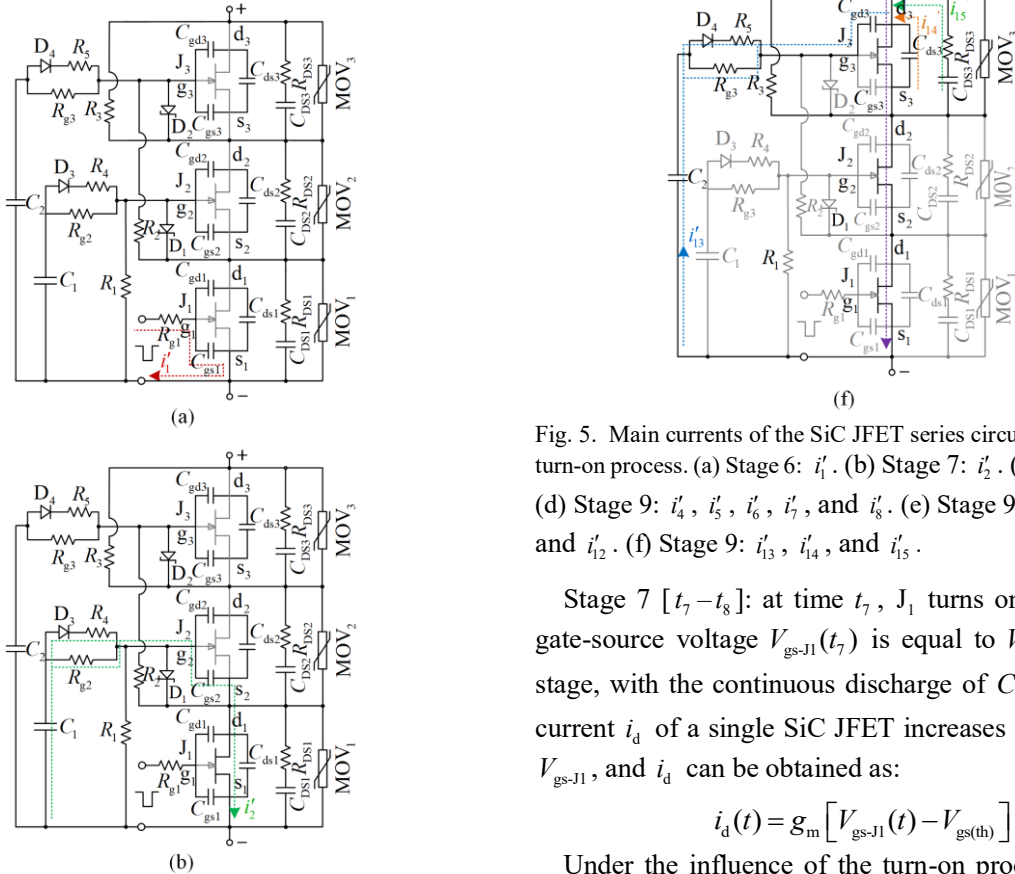


Fig. 5. Main currents of the SiC JFET series circuit during the turn-on process. (a) Stage 6:  $i'_1$ . (b) Stage 7:  $i'_2$ . (c) Stage 8:  $i'_3$ . (d) Stage 9:  $i'_4$ ,  $i'_5$ ,  $i'_6$ ,  $i'_7$ , and  $i'_8$ . (e) Stage 9:  $i'_9$ ,  $i'_{10}$ ,  $i'_{11}$ , and  $i'_{12}$ . (f) Stage 9:  $i'_{13}$ ,  $i'_{14}$ , and  $i'_{15}$ .

Stage 7 [ $t_7 - t_8$ ]: at time  $t_7$ ,  $J_1$  turns on because its gate-source voltage  $V_{gs-J1}(t_7)$  is equal to  $V_{gs(th)}$ . In this stage, with the continuous discharge of  $C_{gs1}$ , the drain current  $i_d$  of a single SiC JFET increases linearly with  $V_{gs-J1}$ , and  $i_d$  can be obtained as:

$$i_d(t) = g_m [V_{gs-J1}(t) - V_{gs(th)}] \quad (11)$$

Under the influence of the turn-on process,  $J_1$ ,  $R_4$ ,

$D_3$ ,  $C_1$ , and  $C_{gs2}$  form a discharge loop in the gate circuit of  $J_2$ . The series branch composed of resistor  $R_4$  and diode  $D_3$  facilitates the acceleration of the discharge of  $C_1$  and  $C_{gs2}$ , thereby promoting the fast turn-on of  $J_2$ . The discharge current  $i_2'$  is shown in Fig. 5(b) and the following relationship exists:

$$V_{C1} + V_{Rg2} + V_{Cgs2} = V_{ds-J1} \quad (12)$$

Consequently, the gate-source voltage  $V_{gs-J2}$  of  $J_2$  gradually increases from  $V_{cc}$ .

Stage 8 [ $t_8 - t_9$ ]: during this stage, the gate-source voltage  $V_{gs-J2}(t_8)$  of  $J_2$  is equal to  $V_{gs(th)}$  at time  $t_8$ ,  $J_3$  remains in the off state. Therefore,  $R_5$ ,  $D_3$ , and  $C_2$  and  $C_{gs3}$  form a discharge loop in the gate circuit of  $J_3$ , and the discharge current  $i_3'$  is shown in Fig. 5(c). Thus, there is:

$$V_{C2} + V_{Rg3} + V_{Cgs3} = V_{ds-J1} + V_{ds-J2} \quad (13)$$

Therefore, the gate-source voltage  $V_{gs-J3}$  gradually increases and reaches the threshold voltage  $V_{gs(th)}$  at time  $t_9$ .

Stage 9 [ $t_9 - t_{10}$ ]: when  $V_{gs-J3} = V_{gs(th)}$ ,  $J_3$  is turned on, and  $I_{D-J1}$ ,  $I_{D-J2}$ , and  $I_{D-J3}$  gradually increase from zero.  $V_{gs-J1}$  reaches the Miller plateau voltage  $V_{gs(mp)}$  at this stage, and therefore,  $V_{ds-J1}$  gradually decreases from one-third of  $V_{bus} \cdot C_{gd1}$ ,  $C_{ds1}$ , and  $C_{DS1}$  begin discharging, and the discharge currents  $i_4'$ ,  $i_5'$ ,  $i_6'$ ,  $i_7'$ , and  $i_8'$  are shown in Fig. 5(d). Owing to the rapid reduction in  $V_{ds-J1}$ ,  $C_1$  in the gate circuit of  $J_2$  accelerates the discharge of  $C_{gs2}$  via  $R_4$  and  $D_3$ . Therefore, the following relationship is obtained:

$$\begin{cases} [(R_{g2} + R_4)/R_{g2}R_4]i_4' + V_{gs-J2} + V_{ds1} = V_{C1} \\ C_1 \frac{dV_{C1}}{dt} = -C_{gs2} \frac{dV_{gs-J2}}{dt} \end{cases} \quad (14)$$

To simplify the calculation, the gate current  $i_4'$  of  $J_2$  is considered to be approximately constant, and (14) can be calculated as:

$$\frac{dV_{gs-J2}}{dt} = -\frac{C_1}{C_1 + C_{gs2}} \frac{dV_{ds-J1}}{dt} \quad (15)$$

Evidently from (15), with a rapid reduction in  $V_{ds-J1}$ , the discharge speed of  $C_{gs2}$  increases, and  $V_{gs-J2}$  gradually increases. When  $V_{gs-J2}$  increases to  $V_{gs(mp)}$ ,  $V_{ds-J2}$  reaches its peak value. Thereafter,  $V_{ds-J2}$  decreases rap-

idly from its maximum value. Simultaneously,  $C_{gd2}$ ,  $C_{ds2}$ , and  $C_{DS2}$  begin discharging, and the discharge currents  $i_9'$ ,  $i_{10}'$ ,  $i_{11}'$ , and  $i_{12}'$  are shown in Fig. 5(e).

Similarly, when  $V_{ds-J2}$  decreases rapidly,  $C_2$  in the gate circuit of  $J_3$  accelerates the discharge of  $C_{gs3}$  via  $R_5$  and  $D_4$  to yield the following:

$$\begin{cases} [(R_{g3} + R_5)/R_{g3}R_5]i_{10}' + V_{gs-J3} + V_{ds-J2} = V_{C2} \\ C_2 \frac{dV_{C2}}{dt} = -C_{gs3} \frac{dV_{gs-J3}}{dt} \end{cases} \quad (16)$$

If the gate current  $i_{10}'$  of  $J_3$  is approximated to be constant, the corresponding solution to (16) can be determined by:

$$\frac{dV_{gs-J3}}{dt} = -\frac{C_2}{C_2 + C_{gs3}} \left( \frac{dV_{ds-J1}}{dt} + \frac{dV_{ds-J2}}{dt} \right) \quad (17)$$

Based on (17), as  $V_{ds-J1}$  and  $V_{ds-J2}$  decrease,  $C_{gs3}$  discharges rapidly, and  $V_{gs-J3}$  gradually increases. Therefore,  $V_{ds-J3}$  reaches its maximum when  $V_{gs-J3}$  is equal to  $V_{gs(mp)}$ . At this stage, the discharge currents  $i_{13}'$ ,  $i_{14}'$ , and  $i_{15}'$  correspond to  $C_{gd3}$ ,  $C_{ds3}$ , and  $C_{DS3}$  respectively, as shown in Fig. 5(f).

Stage 10 [ $t_{10} - t_{11}$ ]: at time  $t_{10}$ ,  $J_1$ ,  $J_2$ , and  $J_3$  are all turned on. The drain-source voltages  $V_{ds-J1}$ ,  $V_{ds-J2}$ , and  $V_{ds-J3}$  all decrease to zero. During this period, influenced by the driving signal  $V_{cc}$ ,  $V_{gs-J1}$  further increases from  $V_{gs(mp)}$  to zero. After the discharging of  $C_1$  and  $C_2$  is complete,  $V_{gs-J2}$  and  $V_{gs-J3}$  further increase from  $V_{gs(mp)}$  to zero. At  $t_{11}$ , the SSCB returns to its normal state.

### III. KEY PARAMETER SETTINGS OF THE SSCB GATE DRIVER

#### A. Parameter Selection of $C_1$ and $C_2$

During the turn-on and turn-off processes of the cascaded SiC JFETs, the bottom device  $J_1$  is driven by a standard single-gate driver, while  $J_2$  and  $J_3$  are driven by the charge transfer between the capacitors in their respective gate circuits. An analysis of the turn-off process for  $J_2$  during Stage 3 is considered as an example. Based on the principle of charge conservation, the following expression is satisfied:

$$C_1 \Delta V_{C1} = C_{gs-J2} \Delta V_{gs-J2} + C_{gd2} \Delta V_{gd-J2} \quad (18)$$

where  $\Delta V_{C1}$  is the voltage variation of  $C_1$ ;  $\Delta V_{gs-J2}$  and  $\Delta V_{gd-J2}$  are the voltage variations of  $C_{gs2}$  and  $C_{gd2}$ , respectively. And the following relationship holds:

$$\begin{cases} V_{C1} = V_{ds-J1} + V_{gs-J2} + V_{Rg2} \\ V_{gd-J2} = V_{gs-J2} - V_{ds-J2} \end{cases} \quad (19)$$

In general, the gate currents of  $J_2$  and  $J_3$  are small, and  $V_{gs-J2}$  and  $V_{gs-J3}$  are maintained within the  $V_{cc}$  range by Zener diodes  $D_1$  and  $D_2$ , respectively. Therefore,  $V_{Rg2}$ ,  $V_{Rg3}$ ,  $V_{gs-J2}$ , and  $V_{gs-J3}$  can be ignored in the approximation. In this case,  $C_1$  and  $C_2$  are approximated as:

$$C_i = \frac{3V_{cc}C_{gs(i+1)} + V_{bus}C_{gd(i+1)}}{3V_{Ci}}, i = 1, 2 \quad (20)$$

According to (19) and (20), the voltage  $V_{C2}$  of  $C_2$  is approximately twice that of  $C_1$  in the steady state. Thus,  $C_1$  has the following option:

$$C_1 \approx 2C_2 \quad (21)$$

### B. Parameter Selection of $R_{g1}$ , $R_{g2}$ and $R_{g3}$

In the gate drive circuit of the SSCB, in addition to the parasitic capacitor  $C_{gs}$  and gate resistor  $R_g$  of the SiC JFET, the equivalent inductance  $L_{eq}$  includes the printed circuit board (PCB) circuit and the parasitic and stray inductances of the device. Together, these parameters form a multi-order system. To reduce the electrical oscillation in the SiC JFET gate circuit, appropriate gate resistors  $R_{g1}$ ,  $R_{g2}$ , and  $R_{g3}$  must be selected to ensure that the corresponding gate circuits operate in an overdamping or critical-damping state. Thus,  $R_{g1}$  conforms to the following relationship:

$$R_{g1} > 2\sqrt{\frac{L_{eq}}{C_{gs1}}} \quad (22)$$

Given that  $C_1$  and  $C_2$  accelerate the turn-on and turn-off speeds of  $J_2$  and  $J_3$ , the gate resistors  $R_{g2}$  and  $R_{g3}$  satisfy the following condition:

$$R_{g(i+1)} > 2\sqrt{\frac{L_{eq}}{C_{gs(i+1)} + C_i}}, i = 1, 2 \quad (23)$$

The larger the equivalent inductance  $L_{eq}$  is, the more significant the oscillation phenomenon appears in the SSCB gate circuit. In the actual PCB design process, if  $R_{g1}$ ,  $R_{g2}$ , and  $R_{g3}$  are as close to the gate pins of the corresponding SiC JFETs as possible, the oscillation can be suppressed.

The resistance values of  $R_{g1}$ ,  $R_{g2}$ , and  $R_{g3}$  determine the rise and fall times of the SiC JFET gate drive signals. To avoid the increase in power consumption caused by long rise and fall times, the minimum conduction time,  $T_{on\_min}$  of the SiC JFET device can be used to approximately determine the maximum values of  $R_{g1}$ ,  $R_{g2}$ , and

$R_{g3}$ . The SiC JFETs used in this study are UJ3N120035K3S, produced by UnitedSiC, and the typical minimum conduction time  $T_{on\_min}$  is approximately 37 ns. Thus,  $R_{g1}$ ,  $R_{g2}$ , and  $R_{g3}$  are approximated by:

$$R_{gi} < \frac{1}{40} \frac{T_{on\_min}}{C_{gsi}}, i = 1, 2, 3 \quad (24)$$

Consequently, to satisfy the requirements of the SSCB for oscillation suppression and rapid response,  $R_{g1}$ ,  $R_{g2}$ , and  $R_{g3}$  should be as small as possible within the allowable range. During the SSCB turn-on process, the maximum dynamic voltage imbalance occurs during the turn-on times of  $J_2$  and  $J_3$ . Using  $R_4$ ,  $R_5$ ,  $D_3$ , and  $D_4$ , the turn-on speeds of  $J_2$  and  $J_3$  can be further improved, and the dynamic voltage imbalance of the cascaded SiC JFETs is reduced.

### C. Influence of Key Parameters on the SSCB

To assess the influence of the gate resistors ( $R_{g1}$ ,  $R_{g2}$ , and  $R_{g3}$ ) and drive capacitors ( $C_1$  and  $C_2$ ) on the switching characteristics of the SSCB, a simulation model of the SiC JFET series circuit shown in Fig. 2 is built using ORCAD/PSpice. The main parameters of the series circuit are listed in Table I. Taking the gate resistor  $R_{g1}$  and the drive capacitor  $C_1$  as examples, the drain-source voltages  $V_{ds1,2,3}$  and gate-source voltages  $V_{gs1,2,3}$  during the turn-off of the cascaded SiC JFETs are observed when the values of  $R_{g1}$  and  $C_1$  are varied. The influence of  $R_{g1}$  and  $C_1$  on the voltage balance of the cascaded SiC JFETs is analyzed and the simulation results are presented in Fig. 6.

TABLE I  
MAIN COMPONENT PARAMETERS IN THE SIMULATION

Parameters	Values
Gate resistor $R_{g1}$	10 $\Omega$
Gate resistor $R_{g2}$ , $R_{g3}$	5 $\Omega$
Gate discharge resistor $R_4$ , $R_5$	0.2 $\Omega$
Gate capacitor $C_1$	500 pF
Gate capacitor $C_2$	200 pF
Snubber capacitors $C_{DS1}$ , $C_{DS2}$ , $C_{DS3}$	2.2 nF
Snubber capacitors $R_{DS1}$ , $R_{DS2}$ , $R_{DS3}$	200 $\Omega$
Voltage balancing resistor $R_1$ , $R_2$ , $R_3$	100 k $\Omega$
SiC JFET (UJ3N120035K3S UnitedSiC)	1.2 kV/63 A
Limit current inductance $L_m$	0.028 mH
DC-bus voltage $V_{bus}$	1.5 kV
Cable $\pi$ -equivalent resistance $R_x$	120 m $\Omega$ /km
Cable $\pi$ -equivalent inductance $L_x$	0.56 mH/km
DC-link capacitor $C_{link}$	5 mF

When  $R_{g1}$  is adjusted,  $R_{g2}$ ,  $R_{g3}$ ,  $C_1$ , and  $C_2$  remain unchanged. The operating conditions for the voltages



$V_{ds1,2,3}$  and  $V_{gs1,2,3}$  are shown in Fig. 6(a). The results indicate that when  $R_{g1}$  increases from  $10 \Omega$  to  $30 \Omega$ , the decrease rate of  $V_{gs1,2,3}$  from 0 to  $-15$  V reduces, and the turn-off times of  $J_1$ ,  $J_2$ , and  $J_3$  are prolonged. However, the drain-source voltages  $V_{ds1,2,3}$  of  $J_1$ ,  $J_2$ , and  $J_3$  are maintained at 500 V after the device is completely turned off. When  $C_1$  increases from 100 pF to 500 pF,  $R_{g1}$ ,  $R_{g2}$ ,  $R_{g3}$ , and  $C_2$  remain unchanged. The voltages  $V_{ds1,2,3}$  and  $V_{gs1,2,3}$  of the cascaded SiC JFETs vary with  $C_1$ , as shown in Fig. 6(b). The simulation results show that the increase in  $C_1$  increases the charging speed of the gate-source capacitor  $C_{gs-J2}$ , and this causes  $V_{gs2}$  to decrease rapidly. This results in a shorter time for  $V_{ds2}$  to increase from 0 to 500 V. Simultaneously, during the charging effect of  $V_{ds2}$  on  $C_{gs-J3}$ , the turn-off speed of  $J_3$  is also improved. However,  $V_{gs1}$  is not affected by  $C_1$ , thus causing  $V_{ds1}$  to be less than 500 V when the cascade SiC JFETs are turned off. Therefore, variation in  $C_1$  has a significant influence on the voltage balance of the cascaded SiC JFETs. These results of the simulation analyses can serve as a reference for the selection of important SSCB parameters.

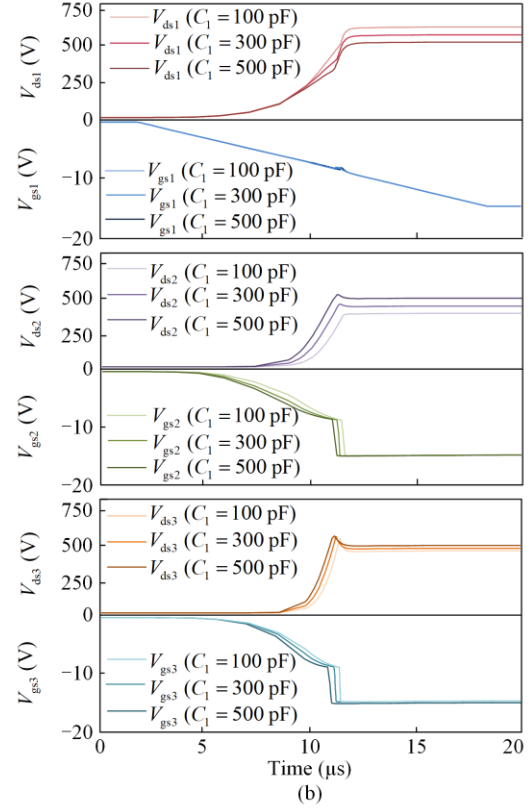
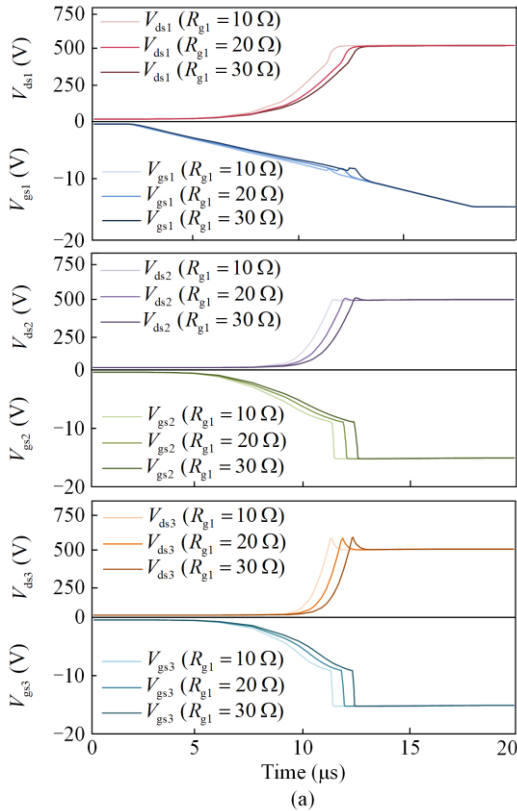


Fig. 6. Simulation results of the SiC JFET series circuit when the values of  $R_{g1}$  and  $C_1$  are varied respectively. (a)  $V_{DS1,2,3}$  and  $V_{gs1,2,3}$  results for a set of different values of  $R_{g1}$ . (b)  $V_{DS1,2,3}$  and  $V_{gs1,2,3}$  results for a set of different capacitances of  $C_1$ .

#### IV. CURRENT LIMITING PROTECTION METHOD FOR SSCB

##### A. Protection Principle of the SSCB

When a fault occurs in a DC distribution network as shown in Fig. 7, the increasing rate and amplitude of the fault current depend primarily on the fault type. Therefore, to better distinguish between the fault types and prevent maloperation of the SSCB, protection is provided according to the fault situation. A flowchart of the SSCB protection method is presented in Fig. 8. The implementation process of the SSCB protection is described in the following sections.

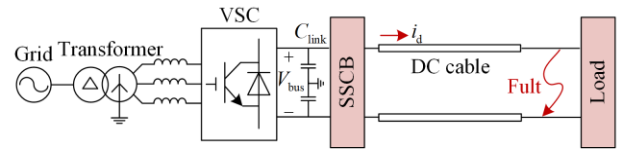


Fig. 7. Schematic of a DC distribution network with the proposed SSCB.

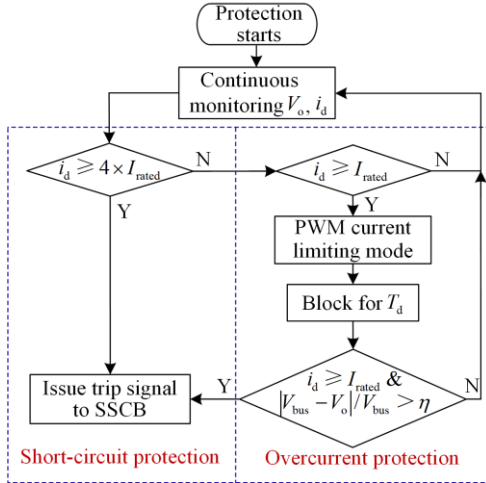


Fig. 8. Flowchart of the current limiting protection method for SSCB.

### 1) Normal Operation

When the current  $i_d$  monitored by the SSCB current-sampling circuit satisfies  $i_d \leq I_{\text{rated}}$  ( $I_{\text{rated}}$  is the SiC JFET nominal current), the SiC JFET series circuit of the SSCB is maintained in the on state, and the DC system operates normally.

### 2) Short-circuit Protection

Generally, short circuits are serious types of faults in DC systems. After a short-circuit fault occurs, the SSCB must isolate the fault before  $i_d$  increases to an unacceptable value. Considering the safety of the SiC JFET device, when  $i_d$  is greater than or equal to  $4I_{\text{rated}}$ , it can be regarded as a short circuit. Here, the microprocessor applies  $-15$  V to the gate of  $J_1$ , thus causing the SSCB to turn off.

### 3) Overcurrent Protection

When  $i_d$  is such that  $I_{\text{rated}} < i_d < 4I_{\text{rated}}$ , an overcurrent event occurs in the DC system. The junction temperature of SiC JFETs continues to increase after a long period of overcurrent. This can cause thermal damage to the SiC JFETs. However, the short-term inrush current generated by capacitive load startup has a minor impact on the safe operation of the DC network, and the SSCB must be maintained in the on state. In this case, the SSCB can prevent maloperation by distinguishing between the overcurrent and the inrush current, thus enhancing the reliability of the SSCB. Therefore, when the SSCB detects that  $i_d$  satisfies  $I_{\text{rated}} < i_d < 4I_{\text{rated}}$ , it adopts a PWM current-limiting mode with the delay time  $T_d$ . This mode is used to limit the time that the SSCB is in an overcurrent state, thereby reducing the thermal stress of the SiC JFETs. The delay time  $T_d$  can be selected according to the maximum thermal capacity of the SiC JFET for different overcurrent values. Reference [16] has already discussed the

relevant theoretical basis for setting  $T_d$  in detail, and thus it is not elaborated further here. Consequently, the SSCB adopts different protection principles for the aforementioned two overcurrent conditions.

1) Overcurrent fault: if  $I_{\text{rated}} < i_d < 4I_{\text{rated}}$ , a PWM control signal is applied to the gate of the cascaded SiC JFETs. After a period of  $T_d$ ,  $I_{\text{rated}} < i_d < 4I_{\text{rated}}$  is still satisfied, while the load voltage  $V_o$  cannot be restored to the normal level  $|V_{\text{bus}} - V_o|/V_{\text{bus}} > \eta$  (in this study,  $\eta$  is set to 10%). Thus, the occurrence of a permanent overcurrent fault in the DC system can be deduced. At this time, the microprocessor sends a negative gate signal  $V_{\text{cc}}$  to the gate of  $J_1$  to turn-off the SSCB.

2) Inrush current: after the SSCB experiences a  $T_d$  period in the PWM mode,  $i_d$  returns to the normal level ( $i_d \leq I_{\text{rated}}$ ), and the load voltage  $V_o$  satisfies the condition  $|V_{\text{bus}} - V_o|/V_{\text{bus}} \leq \eta$ .  $i_d$  is considered to be an inrush current generated during capacitive load startup, and therefore the SSCB returns to its normal on state.

### B. Simulation Results for SSCB

The simulation model corresponding to Fig. 7 is developed in PSCAD/EMTDC to evaluate the effectiveness of the proposed SSCB protection method for different DC fault types, while the system parameters were presented in Table I. The SSCB simulation waveforms when the short-circuit fault, overcurrent, and inrush current occurred are shown in Fig. 9.

The simulation results of the DC-bus voltage  $V_{\text{bus}}$ , drain-source voltage  $V_{\text{DS}}$  and drain current  $i_d$  of the SSCB during the short-circuit fault are shown in Fig. 9(a). As seen, at 0.9 ms,  $i_d$  is increased sharply after the short-circuit fault. When  $i_d$  reaches 4 times the SiC JFET nominal current, the SSCB responds to the short-circuit fault and finally completes fault isolation. As shown in Fig. 9(b), when a permanent overcurrent fault occurs in the DC system at 0.9 ms,  $i_d$  increases rapidly from 25 A to approximately 130 A. To determine whether  $i_d$  is a permanent overcurrent, the SSCB enters into the PWM current-limiting mode with a delay time of 1.8 ms. At the end of the current limiting mode,  $i_d$  is still greater than the SiC JFET nominal current (63 A) while  $V_o$  satisfies the inequality  $|V_{\text{bus}} - V_o|/V_{\text{bus}} > 10\%$ . At this time, to prevent thermal damage to the SiC JFETs owing to the continuous overcurrent, the SSCB is turned off, and overcurrent protection is achieved. Fig. 9(c) shows the waveforms for the SSCB when an inrush current is generated by the capacitive load. Evidently, when the DC system operates normally,  $i_d$  is 25 A. At 0.9 ms, capacitive loading occurs in the DC system, and  $i_d$  increases rapidly from 25 A to approximately 125 A. In this case, the SSCB also enters into PWM current-limiting mode. After

a delay time  $T_d$  of 1.8 ms,  $i_d$  is less than the rated current of 63 A, while  $V_o$  satisfies the inequality  $|V_{bus} - V_o|/V_{bus} \leq 10\%$ . The SSCB is then switched to the on state.

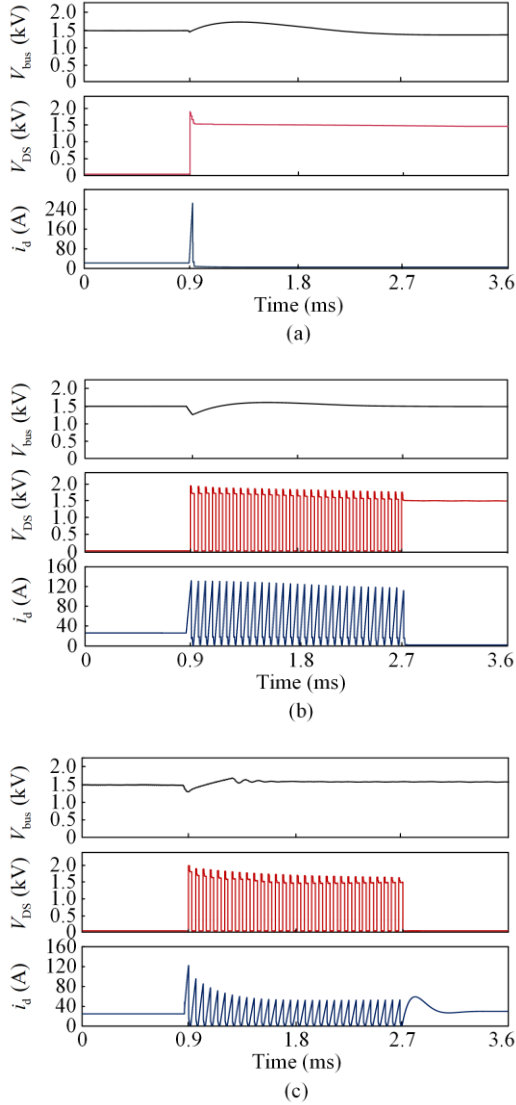


Fig. 9. Simulation waveforms of the SSCB when short-circuit fault, overcurrent, and inrush current occurred. (a)  $V_{bus}$ ,  $V_{DS}$ , and  $i_d$  results for a short-circuit fault. (b)  $V_{bus}$ ,  $V_{DS}$ , and  $i_d$  results for an overcurrent. (c)  $V_{bus}$ ,  $V_{DS}$ , and  $i_d$  results for an inrush current.

## V. EXPERIMENTAL RESULTS

As shown in Fig. 10(a), to experimentally evaluate the effectiveness of the proposed topology, a 1.5 kV, 63 A SSCB prototype based on three cascaded normally-on SiC JFETs has been developed. Figs. 11 and 10(b) show the simplified schematic and image of the fault test set-up, respectively. Tests are performed at a maximum DC voltage of 750 V, and the key parameters of the SSCB prototype and the test set-up are listed in Table II.

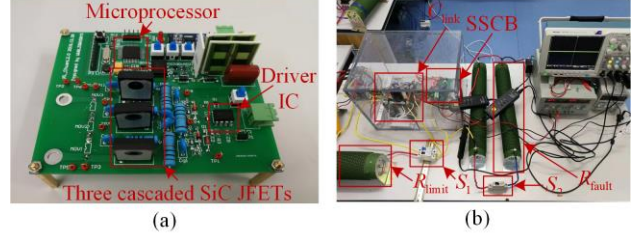


Fig. 10. Image of the designed SSCB prototype and DC fault test set-up. (a) SSCB prototype. (b) Test set-up.

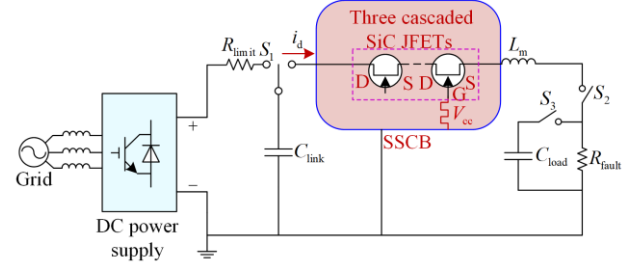


Fig. 11. Simplified schematic of DC fault test set-up.

TABLE II  
ELECTRICAL PARAMETERS OF THE SSCB PROTOTYPE  
AND THE TEST SET-UP

Parameters	Values
Gate resistor $R_{g1}$	10 $\Omega$
Gate resistor $R_{g2}$ , $R_{g3}$	5 $\Omega$
Gate discharge resistor $R_4$ , $R_5$	0.2 $\Omega$
Gate capacitor $C_1$	470 pF
Gate capacitor $C_2$	220 pF
Snubber capacitors $C_{DS1}$ , $C_{DS2}$ , $C_{DS3}$	2.2 nF
Snubber capacitors $R_{DS1}$ , $R_{DS2}$ , $R_{DS3}$	200 $\Omega$
Voltage balancing resistor $R_1$ , $R_2$ , $R_3$	100 k $\Omega$
Microprocessor	STM8S105
SiC JFET (UJ3N120035K3S UnitedSiC)	1.2 kV/63 A
DC-link capacitor $C_{link}$	2.2 mF
Load capacitor of test setup $C_{load}$	100 $\mu$ F
Limit resistor of test setup $R_{limit}$	100 $\Omega$
Limit current inductance $L_m$	0.028 mH

### A. Short-circuit Experimental Results

In the test set-up, switch  $S_1$  is used to connect the DC-link capacitor  $C_{link}$  to the DC power supply to charge the voltage  $V_{bus}$  of  $C_{link}$  to 750 V. Then,  $C_{link}$  is connected to the SSCB through  $S_1$  for the subsequent short-circuit fault test. Therefore, when  $S_2$  is closed, the dynamic response of the proposed SSCB is tested for a short-circuit fault, while the fault resistance  $R_{fault}$  is set to 3  $\Omega$ .

Figure 12 shows the SSCB experimental waveforms obtained during the short-circuit fault isolation process.

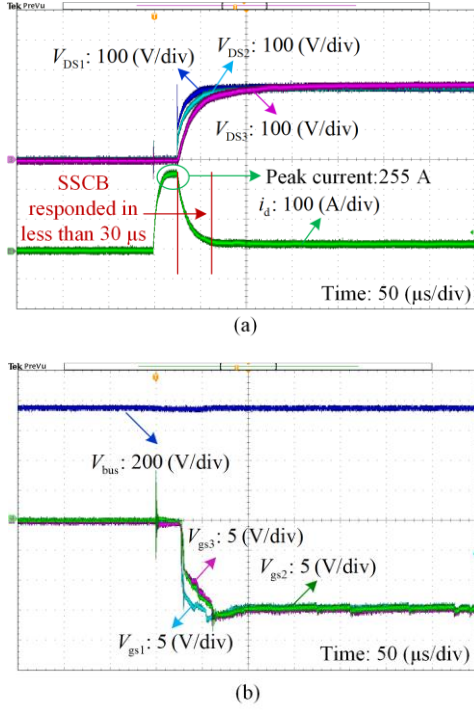


Fig. 12. Experimental waveforms of the SSCB during a short-circuit fault isolation process. (a) Drain-source voltages  $V_{DS1}$ ,  $V_{DS2}$  and  $V_{DS3}$  and short-circuit current  $i_d$ . (b) Gate-source voltages  $V_{gs1}$ ,  $V_{gs2}$  and  $V_{gs3}$  and DC-link voltage  $V_{bus}$ .

As shown in Fig. 12(a), when a short-circuit fault occurs, the current  $i_d$  flowing through the cascaded SiC JFETs ( $J_1$ ,  $J_2$ , and  $J_3$ ) of the SSCB rapidly increases from zero to 255 A (approximately 4 times the SiC JFET nominal current). At this point, the SSCB gate driver responds rapidly to the fault. The microprocessor sends a bias voltage of  $-15$  V to the gate of  $J_1$ . The gate-source voltages  $V_{gs1}$ ,  $V_{gs2}$ , and  $V_{gs3}$  of  $J_1$ ,  $J_2$ , and  $J_3$  reduce from zero to  $-15$  V, respectively, as shown in Fig. 12(b). Thus, the SiC JFETs are turned off individually, and the action response time of the SSCB is approximately 30  $\mu$ s. During the SSCB turn-off process, the drain-source voltages  $V_{DS1}$ ,  $V_{DS2}$ , and  $V_{DS3}$  of the cascaded SiC JFETs successively increase from zero to approximately 250 V, as shown in Fig. 12(a), with no overvoltage observed. When the SSCB is completely turned off,  $V_{DS1}$ ,  $V_{DS2}$ , and  $V_{DS3}$  are maintained at approximately 250 V. Thus a balanced distribution of the drain-source voltages in the SiC JFET series circuit is realized.

### B. Overcurrent Experimental Results

To evaluate the SSCB performance for an overcurrent event, the voltage  $V_{bus}$  is also 750 V while the resistance  $R_{fault}$  is set to 6  $\Omega$ . Therefore, when  $S_2$  is closed, an overcurrent is simulated. From the maximum thermal capacity of the SiC JFET for different over-

current values, the PWM current-limiting delay interval  $T_d$  is set to 1.8 ms when the overcurrent is twice that of the SiC JFET nominal current.

Figure 13 shows the SSCB experimental waveforms for the overcurrent event. It shows that when  $S_2$  is turned on,  $i_d$  quickly increases from zero to 130 A (approximately twice the SiC JFET nominal current). Based on the overcurrent protection principle, to effectively determine whether  $i_d$  is a persistent overcurrent or an inrush current generated by capacitive load startup, the microprocessor sends a PWM control signal with a delay interval of 1.8 ms to the gate of  $J_1$ . At the end of the PWM mode,  $i_d$  is still larger than the SiC JFET nominal current (63 A), while the load voltage  $V_o$  is approximately 660 V, which satisfies the inequality  $|V_{bus} - V_o|/V_{bus} > 10\%$ . Therefore, the SSCB infers that  $i_d$  is an overcurrent, and the microprocessor sends a bias voltage signal ( $-15$  V) to the gate of  $J_1$  to turn off the SSCB. Thus, the overcurrent protection of the SSCB is realized. Figure 13 shows that when the SSCB is turned off, the overvoltage suppression effect of the drain-source voltages  $V_{DS1}$ ,  $V_{DS2}$ , and  $V_{DS3}$  of  $J_1$ ,  $J_2$ , and  $J_3$  are optimal. Simultaneously, the designed SSCB achieves balanced dynamic and static distributions of the drain-source voltages of the SiC JFETs.

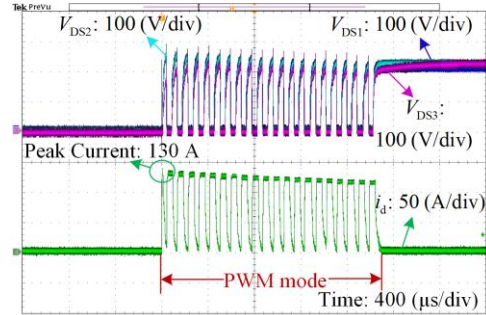


Fig. 13. Experimental waveforms of the SSCB for an overcurrent event.

### C. Inrush Current Experimental Results

For the test circuit shown in Fig. 11, if  $C_{load}$  (100  $\mu$ F) is connected in parallel at both ends of the fault resistance  $R_{fault}$  (20  $\Omega$ ) with  $S_3$ , the inrush current caused by the capacitive load startup can be simulated by controlling  $S_3$ . In this test,  $V_{bus}$  is also set to 750 V.

Figure 14 gives the test waveforms of the SSCB for the capacitive load event. After the capacitive load starts up, the inrush current  $i_d$ , owing to the influence of the capacitor  $C_{load}$ , increases rapidly from 0 to approximately 120 A. Similarly, to determine whether  $i_d$  is caused by an overcurrent fault or capacitive load operation, the SSCB

enters into the PWM mode with a delay of 1.8 ms. During the PWM mode, the charging process of  $C_{load}$  is gradually completed. When the PWM mode ends,  $i_d$  decreases to approximately 37 A, which is within the operating range of the SiC JFET nominal current. At this point, voltage  $V_o$  also satisfies the inequality  $|V_{bus} - V_o|/V_{bus} \leq 10\%$ . The SSCB infers that  $i_d$  is the inrush current generated during normal capacitive load startup. Therefore, a 0 V drive signal is applied to the gate of the SiC JFETs to enable the SSCB to operate normally.

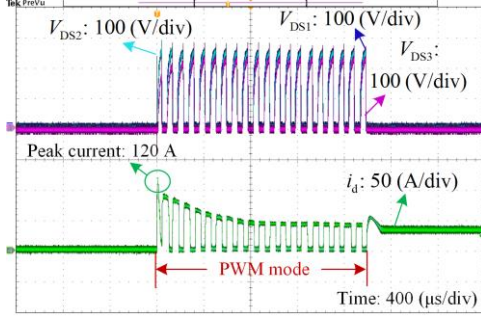


Fig. 14. Experimental results of the SSCB during an inrush current condition.

#### D. Fault Recovery Experimental Results

After a fault in the DC system is removed, the SSCB is turned on and the DC distribution system resumes normal operation. Figure 15 shows the experimental waveforms of the SSCB during the turn-on process.

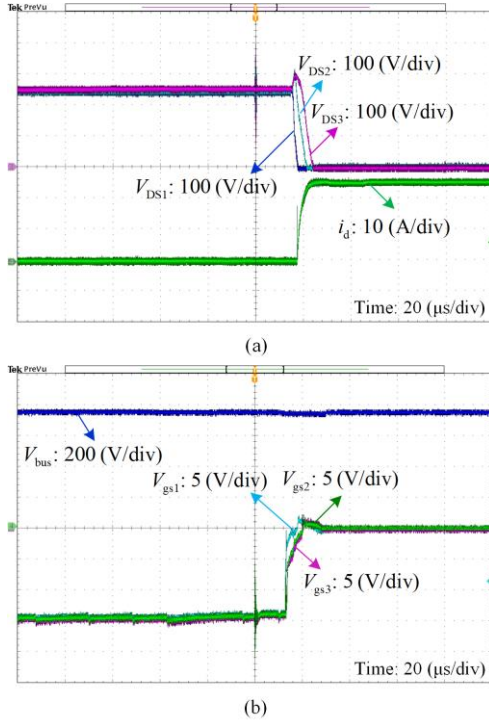


Fig. 15. Experimental waveforms obtained when the SSCB is restored to normal operation. (a) Drain-source voltages  $V_{DS1}$ ,  $V_{DS2}$  and  $V_{DS3}$  and load current  $i_d$ . (b) Gate-source voltages  $V_{gs1}$ ,  $V_{gs2}$  and  $V_{gs3}$  and DC-link voltage  $V_{bus}$ .

The voltage  $V_{bus}$  and load resistance  $R_{fault}$  are set to 750 V and 30  $\Omega$ , respectively. As shown in Fig. 15(b), when the DC fault is removed, the SSCB drive circuit sends a turn-on signal (0 V) to the gate of  $J_1$ . At this time, the gate-source voltage  $V_{gs1}$  of  $J_1$  increases from -15 V to zero, i.e.,  $J_1$  is switched from the off state to the on state. Therefore, the drain-source voltage  $V_{DS1}$  of  $J_1$  gradually decreases from 250 V to zero, as shown in Fig. 15(a). During the turn-on process of  $J_1$ ,  $J_2$  and  $J_3$  are turned on individually, and the corresponding drain-source voltages  $V_{DS2}$  and  $V_{DS3}$  are gradually reduced from 250 V to zero. The load current  $i_d$  also increases from zero to approximately 25 A. The drain-source voltages  $V_{DS1}$ ,  $V_{DS2}$ , and  $V_{DS3}$  do not exhibit significant overshoots during the SSCB turn-on process. The time required for the SSCB to be fully turned on is under 20  $\mu$ s.

## VI. CONCLUSION

To fulfill the requirements of SiC-based SSCB applications at medium-voltage level, the series operation of solid-state SiC devices is an economical and feasible way to improve their applicability. In this study, a 1.5 kV, 63 A medium-voltage SSCB based on cascaded normally-on SiC JFETs is presented. The SSCB consists of three main components: a signal sampling circuit, a microprocessor control unit, and a main static switch composed of three SiC JFETs in series. A programmable gate driver design facilitates good dynamic and static voltage sharing of the SiC JFETs during series operation, thus effectively suppressing the overvoltage during the turn-on and turn-off processes of the SSCB. The key parameters and selection conditions of the SSCB gate driver are analyzed, thus providing a useful reference for the practical design of an SSCB for medium-voltage DC distribution protection. Additionally, an improved PWM current-limiting protection approach is presented to realize fast short-circuit and overcurrent protection, and to avoid maloperation of the SSCB owing to the transient inrush current. The proposed method is validated based on interruption tests of an SSCB prototype. The test results reveal that the designed SSCB achieves reliable protection against different fault conditions and is effective for the series operation of SiC devices. This has important practical significance in ensuring the safe and stable operation of medium-voltage DC distribution networks.

## ACKNOWLEDGMENT

Not applicable.

#### AUTHORS' CONTRIBUTIONS

**Dong He:** proposed the innovative points and drafted the original manuscript. **Haohui Zhou:** analyzed the data and contributed to writing the original draft of the manuscript. **Zheng Lan:** contributed to writing the original draft of the manuscript. **Wei Wang:** investigated the voltage equalization method and research background of medium-voltage SSCBs. **Jinhui Zeng:** conducted experiments and verified the accuracy of the results. **Xueping Yu:** checked and revised English expression. **Z. John Shen:** provided theoretical guidance. All authors read and approved the final manuscript.

#### FUNDING

This work is supported in part by Hunan Provincial Natural Science Foundation of China (No. 2021JJ40172).

#### AVAILABILITY OF DATA AND MATERIALS

Not applicable.

#### DECLARATIONS

Competing interests: The authors declare that they have no known competing financial interests or personal relationships that could have appeared to influence the work reported in this article.

#### AUTHORS' INFORMATION

**Dong He** received the B.S. degree in electrical engineering from the Chongqing University of Posts and Telecommunications, Chongqing, China, in 2010, and the M.S. degree in electrical engineering from the Xiangtan University, Xiangtan, China, in 2014. The Ph.D. degree was received in electrical engineering with the College of Electrical and Information Engineering, Hunan University, Changsha, China, in 2019. He is currently working as an assistant professor with the Hunan University of Technology, Zhuzhou, China. His research interests include solid-state circuit breaker and fault protection technologies of dc microgrid systems.

**Haohui Zhou** received the B.S. degree in electrical engineering and automation from Henan Polytechnic University, Jiaozuo, China, in 2018. He is currently pursuing the M.S. degree in electrical engineering with the College of Electrical and Information Engineering from Hunan University of Technology, Zhuzhou, China. His research interests include fault protection of dc distribution network and design of solid-state circuit breaker.

**Zheng Lan** received the M.S. and Ph.D. degree from the College of Electrical and Information Engineering, Hunan University, Changsha, China, in 2011 and 2017,

respectively. He has been at Hunan University of Technology, as an associate professor since 2022. His research interests include power quality control, solid-state transformer, and distributed power generation technology.

**Wei Wang** received the B.S. degree in electrical engineering and automation from Hunan University, Changsha, China, in 2018, and he is currently pursuing the Ph.D. degree in electrical engineering with the College of Electrical and Information Engineering from Hunan University, Changsha, China. His current research interests include fault analysis of dc distribution networks and design of solid-state protection switch.

**Jinhui Zeng** received the M.S. and Ph.D. degrees in electrical engineering from the College of Electrical and Information Engineering, Hunan University, Changsha, China, in 2009 and 2013, respectively. Since 2019, he has been an associate professor with the Hunan University of Technology. His research interests include power electronic transformation, power quality control, and control methods of renewable energy grid connections.

**Xueping Yu** received the B.S. degree in electrical engineering and automation from the College of Electrical Engineering, Three Gorges University, Yi Chang, China, in 2013, the M.S. degree in electrical engineering from the College of Electrical Engineering, Wuhan University, Wuhan, China, in 2015, and the Ph.D. degree in electrical engineering from Hunan University, Changsha, China, in 2021. She is currently working as an assistant professor with the Hunan University of Technology, Zhuzhou, China. Her research interests include multiport dc converters and the application of power electronics technology in power systems.

**Z. John Shen** received B.S. degree from Tsinghua University, Beijing, China, in 1987, and the M.S. and Ph.D. degrees from the Rensselaer Polytechnic Institute, Troy, NY, USA, in 1991 and 1994, respectively, all in electrical engineering. He was in faculty of the University of Michigan-Dearborn between 1999 and 2004, and the University of Central Florida between 2004 and 2012. In 2013, he joined the Illinois Institute of Technology as the Grainger Chair Professor in electrical and power engineering. Since 2007, he has been holding a courtesy professorship at Hunan University, Changsha, China, and at Zhejiang University, Hangzhou, China since 2013. His research interests include power electronics, power semiconductor devices, etc. Dr. Shen has been an active volunteer in the IEEE Power Electronics Society, and has served as the VP of Products 2009-2012, Associate Editor, and Guest Editor-in-Chief of the IEEE transactions on Power Electronics, Tech-

nical Program Chair and General Chair of several major IEEE conferences.

#### REFERENCES

- [1] Y. Peng, Z. Shuai, and J. M. Guerrero *et al.*, "Performance improvement of the unbalanced voltage compensation in islanded microgrid based on small-signal analysis," *IEEE Transactions on Industrial Electronics*, vol. 67, no. 7, pp. 5531-5542, Jul. 2020.
- [2] J. Hou, G. Song, and Y. Fan, "Fault identification scheme for protection and adaptive reclosing in a hybrid multi-terminal HVDC system," *Protection and Control of Modern Power Systems*, vol. 8, no. 2, pp. 1-17, Apr. 2023.
- [3] G. AlLee and W. Tschudi, "Edison redux: 380 Vdc brings reliability and efficiency to sustainable data centers," *IEEE Power and Energy Magazine*, vol. 10, no. 6, pp. 50-59, Oct. 2012.
- [4] Z. Shuai, D. He, and Z. Xiong *et al.*, "Comparative study of short-circuit fault characteristics for VSC-based DC distribution networks with different distributed generators," *IEEE Journal of Emerging and Selected Topics in Power Electronics*, vol. 7, no. 1, pp. 528-540, Mar. 2019.
- [5] G. Xu, L. Shao, and X. Xu *et al.*, "Degradation state analysis of the IGBT module based on apparent junction temperature," *Protection and Control of Modern Power Systems*, vol. 8, no. 4, pp. 1-14, Oct. 2023.
- [6] Y. Wang, W. Li, and X. Wu *et al.*, "A novel bidirectional solid-state circuit breaker for DC microgrid," *IEEE Transactions on Industrial Electronics*, vol. 66, no. 7, pp. 5707-5714, Jul. 2019.
- [7] R. Rodrigues, Y. Du, and A. Antoniazzi *et al.*, "A review of solid-state circuit breakers," *IEEE Transactions on Industrial Electronics*, vol. 36, no. 1, pp. 364-377, Jan. 2021.
- [8] Z. J. Shen, G. Sabui, and Z. Miao *et al.*, "Wide-bandgap solid-state circuit breakers for DC power systems: device and circuit considerations," *IEEE Transactions on Electron Devices*, vol. 62, no. 2, pp. 294-300, Feb. 2015.
- [9] J. Wei, S. Liu, and J. Tong *et al.*, "Understanding short-circuit failure mechanism of double-trench SiC power MOSFETs," *IEEE Transactions on Electron Devices*, vol. 67, no. 12, pp. 5593-5599, Dec. 2020.
- [10] Y. Zhou, R. Na, and Y. Feng *et al.*, "GaN-based tri-mode intelligent solid-state circuit breakers for low-voltage DC power networks," *IEEE Transactions on Power Electronics*, vol. 36, no. 6, pp. 6596-6607, Jun. 2021.
- [11] Y. Sato, Y. Tanaka, and A. Fukui *et al.*, "SiC-SIT circuit breakers with controllable interruption voltage for 400 V DC distribution systems," *IEEE Transactions on Power Electronics*, vol. 29, no. 5, pp. 2597-2605, May 2014.
- [12] D. P. Urciuoli, D. Ibitayo, and G. Koebke *et al.*, "A compact 100 A, 850 V, silicon carbide solid-state DC circuit breaker," in *2016 IEEE Energy Conversion Congress and Exposition*, Milwaukee, USA, Sept. 2016, pp. 1-5.
- [13] D. P. Urciuoli, V. Veliadis, and H. C. Ha *et al.*, "Demonstration of a 600 V, 60 A, bidirectional silicon carbide solid-state circuit breaker," in *2011 Twenty-Sixth Annual IEEE Applied Power Electronics Conference and Exposition*, Fort Worth, USA, Mar. 2011, pp. 354-358.
- [14] F. Gu'edon, S. K. Singh, and R. A. McMahon *et al.*, "Gate driver for SiC JFETs with protection against normally-on behaviour induced fault," *Electronics Letters*, vol. 47, no. 6, pp. 375-377, Mar. 2011.
- [15] D. He, Z. Xiong, and Z. Lei *et al.*, "Design optimisation of self-powered gate driver for ultra-fast DC solid-state circuit breakers using SiC JFETs," *IET Power Electronics*, vol. 10, no. 15, pp. 2149-2156, Dec. 2017.
- [16] D. He, Z. Shuai, and Z. Lei *et al.*, "A SiC JFET-based solid state circuit breaker with digitally controlled current-time profiles," *IEEE Journal of Emerging and Selected Topics in Power Electronics*, vol. 7, no. 3, pp. 1556-1565, Sept. 2019.
- [17] Y. Ren, X. Yang, and F. Zhang *et al.*, "A compact gate control and voltage-balancing circuit for series-connected SiC MOSFETs and its application in a DC breaker," *IEEE Transactions on Industrial Electronics*, vol. 64, no. 10, pp. 8299-8309, Oct. 2017.
- [18] J. Biela, D. Aggeler, and D. Bortis *et al.*, "Balancing circuit for a 5 kV/50 ns pulsed-power switch based on SiC-JFET super cascade," *IEEE Transactions on Plasma Science*, vol. 40, no. 10, pp. 2554-2560, Oct. 2012.
- [19] X. Wu, S. Cheng, and Q. Xiao *et al.*, "A 3600 V/80 A series-parallel-connected silicon carbide MOSFETs module with a single external gate driver," *IEEE Transactions on Power Electronics*, vol. 29, no. 5, pp. 2296-2306, May 2014.
- [20] F. Zhang, X. Yang, and W. Chen *et al.*, "Voltage balancing control of series-connected SiC MOSFETs by using energy recovery snubber circuits," *IEEE Transactions on Power Electronics*, vol. 35, no. 10, pp. 10200-10212, Oct. 2020.
- [21] A. M. Roshandeh, Z. Miao, and Z. A. Danyial *et al.*, "Cascaded operation of SiC JFETs in medium voltage solid state circuit breakers," in *2016 IEEE Energy Conversion Congress and Exposition*, Milwaukee, USA, Sept. 2016, pp. 1-6.
- [22] H. Duan, W. Wang, and Z. Shuai *et al.*, "A SiC JFETs modular cascaded method with active clamp control strategy for DC solid-state circuit breaker," *CSEE Journal of Power and Energy Systems*, vol. 9, no. 6, pp. 2435-2446, Nov. 2023.
- [23] W. Wang, Z. Shuai, and H. Duan *et al.*, "A single-drive SiC-JFET-SCM for solid state circuit breaker in MVDC distribution networks," *IEEE Transactions on Industrial Electronics*, vol. 70, no. 11, pp. 11121-11131, Nov. 2023.
- [24] D. He, Z. Shuai, and W. Wang *et al.*, "A 2 kV intelligent DC solid state circuit breaker using series connected SiC JFETs," in *2019 IEEE Energy Conversion Congress and Exposition*, Baltimore, USA, Nov. 2019, pp. 1114-1119.